JGR Biogeosciences

RESEARCH ARTICLE
10.1029/2025JG009016

White Is a New Shade of Blue Carbon: A Case Study of a Traditional Salt Production Pond That is a Net Carbon Sink

Ana Alexandre[1], Carmen B. de los Santos[1,2], Javier Jiménez Herrero[1], Alizé Deguette[1], João Silva[1], Márcio Martins[1], Filipe Parreira[1], Nadine Schubert[1], Saray P. de la Rosa[1], and Rui Santos[1]

[1]Grupo de Ecologia de Plantas Marinhas, Centro de Ciências do Mar do Algarve (CCMAR/CIMAR LA), Campus de Gambelas, Universidade do Algarve, Faro, Portugal, [2]Now at Institute of Marine Sciences of Andalusia (ICMAN), Spanish National Research Council (CSIC), Cádiz, Spain

Key Points:

- The potential of salterns as carbon sinks or sources was addressed for the first time by assessing the annual carbon budget
- Diel, seasonal and spatial variability in air-water CH_4 and CO_2 fluxes were determined and integrated with sediment C burial rates
- The substantial amount of C sequestered in the sediments renders the whole saltern a relevant C sink

Supporting Information:

Supporting Information may be found in the online version of this article.

Correspondence to:

A. Alexandre,
aalexandre@ualg.pt

Citation:

Alexandre, A., de los Santos, C. B., Herrero, J. J., Deguette, A., Silva, J., Martins, M., et al. (2026). White is a new shade of blue carbon: A case study of a traditional salt production pond that is a net carbon sink. *Journal of Geophysical Research: Biogeosciences*, *131*, e2025JG009016. https://doi.org/10.1029/2025JG009016

Received 21 APR 2025
Accepted 22 APR 2026

Author Contributions:

Conceptualization: Ana Alexandre, Rui Santos
Data curation: Carmen B. de los Santos
Formal analysis: Ana Alexandre, Carmen B. de los Santos
Funding acquisition: Rui Santos
Investigation: Ana Alexandre, Carmen B. de los Santos, Javier Jiménez Herrero, Alizé Deguette, João Silva, Márcio Martins, Filipe Parreira, Nadine Schubert, Saray P. de la Rosa, Rui Santos
Visualization: Ana Alexandre, Carmen B. de los Santos

Abstract To address for the first time the carbon budget of traditional salterns, we measured the diel, seasonal, and spatial variability of water-air CO_2-eq fluxes (CH_4 and CO_2) and the Organic Carbon (OC) stock and burial rate in the sediment. Temperature, salinity, dissolved oxygen, pH and wind were assessed as potential environmental drivers of the fluxes. The saltern emitted CH_4 to the atmosphere throughout the year, with no significant differences among sites or seasons. On the contrary, the saltern were a sink of CO_2 in summer, autumn and winter, and a source of CO_2 in spring. Water temperature was the main positively related predictor variable of CH_4 fluxes, explaining 29% of their variance, whereas CO_2 fluxes were significantly negatively related to the concentration of O_2 and pH in the seawater and positively related to wind, which explained 66% of fluxes variance. The sedimentary and OC stocks and burial rates were not significantly different among the sampled ponds and averaged 11.9 ± 2.2 Mg OC ha^{-1} and 0.011 ± 0.004 Mg OC ha^{-1} yr^{-1}, respectively. The carbon budget of the saltern was −35.0 g CO_2-eq m^{-2} yr^{-1}, corresponding to −1.49 Mg CO_2-eq yr^{-1} for the total saltern area. This suggests that the-salt industry may function as a carbon sink as opposed to other coastal industries such as fish and shrimp aquaculture. Future studies with additional measurements across a wider range of salterns are needed to evaluate the relevance of "white carbon."

Plain Language Summary Salterns store carbon in their sediments. At the same time, they release carbon from the water to the atmosphere as methane and carbon dioxide, two gases that contribute to global warming. In this study, we evaluated for the first time whether salt ponds are sinks or sources of carbon. We assessed the daily and seasonal fluxes between air and water in a traditional saltern and the amount of carbon that can be stored in the pond sediments. We found that the salt pond had a net capture of CO_2 from the atmosphere to the water in spring, autumn and winter, and that the carbon stored in the sediments was substantial. On an annual basis, the amount of carbon captured in both water and sediments largely exceeded the methane emissions, rendering the whole pond area a relevant carbon sink. Our results highlight the important role of salterns in the global carbon budget and show how they can contribute to mitigate climate change.

1. Introduction

Traditional salt production ponds are human-made basins located in the transition zone between land and sea designed for extracting salt from seawater through the process of solar evaporation. They consist of a series of interconnected shallow ponds through which seawater flows and evaporates by the action of wind and solar energy to become increasingly salty, leading to the final crystallization ponds, where salt precipitates out and can be harvested. Besides salt provision for human consumption, salterns provide relevant ecosystem services such as the support of biodiversity (Takekawa et al., 2006) and particularly of migratory and resident birds as resting and feeding places (Soares et al., 2018; Sripanomyom et al., 2011; Susano & Gonçalves, 2020).

As the water entering the salt pond system does not return to the sea, a substantial part of the organic matter (OM) produced within the ponds is buried in the bottom and may contribute to coastal carbon sequestration and climate change mitigation such as the blue carbon ecosystems (Lovelock & Duarte, 2019). As salterns support high densities of birds, their droppings fertilize the salt ponds (Ganning & Wulff, 1969) fueling primary production and thus, the potential for OM burial. On the other hand, there is the potential for salterns to be sources of carbon to the atmosphere as the accumulation of OM in their sediments drives microbial metabolism, releasing CO_2 and CH_4 as end products (Keneally et al., 2024). Water to air CH_4 emissions have been measured in water-saturated

Writing – original draft: Ana Alexandre, Carmen B. de los Santos, Márcio Martins
Writing – review & editing: Carmen B. de los Santos, Javier Jiménez Herrero, Alizé Deguette, João Silva, Márcio Martins, Filipe Parreira, Nadine Schubert, Saray P. de la Rosa, Rui Santos

sediments and unrestored former industrial salt ponds (490.5–1,607.1 μmol m^{-2} d^{-1}), and in restored salt ponds (4.4–41.4 μmol m^{-2} d^{-1}), in contrast with salt marshes (−24.3 to −1.7 μmol m^{-2} d^{-1}), that were net CH_4 sinks (Zhou et al., 2021). The scarce available evidence suggests that the amount of Organic Carbon (OC) stored in active salterns can be quite high, with values only slightly lower than natural salt marshes (700 vs. 900 Mg CO_2 ha^{-1}) (Díaz-Almela et al., 2019).

To elucidate whether salterns are carbon sources or sinks, it is necessary to assess the carbon budget based on the main processes of carbon dynamics in the salt ponds. The net carbon budget is mostly determined by the balance between (a) carbon dioxide transfer from the atmosphere to the water column, (b) the OC transfer from the water to the sediment (carbon sequestration or burial), and (c) carbon transfer from the water column back to the atmosphere resulting from OM decomposition (CO_2 and CH_4). Other carbon transfers into the salt pond system are associated with the water income from the lagoon, particularly in the summer when evaporation is high, and from OM detritus, rain and dust. When this balance is positive, the system functions as a carbon source; otherwise, it acts as a carbon sink (Bianchi, 2007). The carbon storage capacity and emissions by salterns are virtually unknown. Considering the large extent, yet to be quantified, global area of salterns, it is of utmost relevance to assess if they are carbon sinks, similar to what was revealed for natural hypersaline tidal flats (Brown et al., 2021).

In this study, we assessed the diel and seasonal variability of the net air-water CH_4 and CO_2 fluxes of an operating traditional salt production facility in Ria Formosa, Southern Portugal, and the key environmental drivers of these fluxes. We also quantified the OC stocks and burial rates within the salt pond sediments. By integrating the discrete measurements of the air-water carbon fluxes with the sediment burial rates, we roughly estimated an annual carbon budget for the salt pond area.

2. Materials and Methods

2.1. Study Site

The study was conducted in the salt ponds of the traditional salt production company Necton (Companhia Portuguesa de Culturas Marinhas, S.A.), located in Olhão, Algarve, South Portugal (37.024°N, −7.869°W) (Figures 1a and 1b). The Algarve region has a semi-arid Mediterranean climate, with a 30-year average (minimum-maximum) annual rainfall of 598 mm (429–1,336 mm) and a mean annual air temperature of 16.2°C (13.8–17.8°C), considering the period from 1991 to 2020 (Instituto Português do Mar e da Atmosfera, Data Clima, 2026). The ponds receive seawater from the adjacent mesotidal Ria Formosa lagoon (Figure 1b).

The salt pond area includes 18 interconnected evaporation ponds, covering a total area of ca. 42,500 m^2 (Figure 1c). The water first enters a decanter pond through a manually operated gate. Then, the water flows by gravity through the evaporation ponds until the crystallizer ponds where the salt precipitates and is collected for commercialization. While progressing through the pond system, the water salinity increases due to evaporation. During this study, the water level inside the ponds varied between 17 and 33 cm.

2.2. CH_4 and CO_2 Flux Measurements

Fluxes of CH_4 and CO_2 were measured in July 2023 (summer), November 2023 (autumn), February 2024 (winter) and May 2024 (spring) at the water-air interface at three sites of the evaporation salt ponds, indicated as F1, F2, and F3 (Figure 1c). Preliminary CH_4 and CO_2 flux measurements were also made in the winter and spring of 2021, which allow a rough assessment of inter-annual variability. Fluxes were measured with a semi-spherical opaque floating chamber (33 cm in diameter, Figure 2), deployed at the water surface at a fixed point on each site and connected via two gas-tight ports in a closed loop to a portable CH_4 and CO_2 analyzer (LGR-ICOS™ M-GGA-918, ABB Inc. Measurement and Analytics). The analyzer measured the gas concentration in the air of the chamber at 5-s intervals, using laser cavity ringdown spectroscopy. Precision was 1 ppb over an operating range of 0–100 ppm for CH_4, and 0.4 ppm over a range of 0–20,000 ppm for CO_2. Flux measurements lasted about 30 min to achieve a linear rate of change in gas concentration over time within the chamber and were repeated at each site at intervals of approximately 2 hr. During the night, the time interval between flux measurements was longer (6–7 hr). Flux measurements were performed until a full 24 hr period was completed, except in autumn when the cycle was interrupted after 13 hr due to adverse weather conditions. In total, 9 to 10 incubations were performed at each site and season over the diel cycle, except for autumn, in which 7 to 8 incubations were performed. Fluxes were calculated following Equation 1 (Brown et al., 2021).

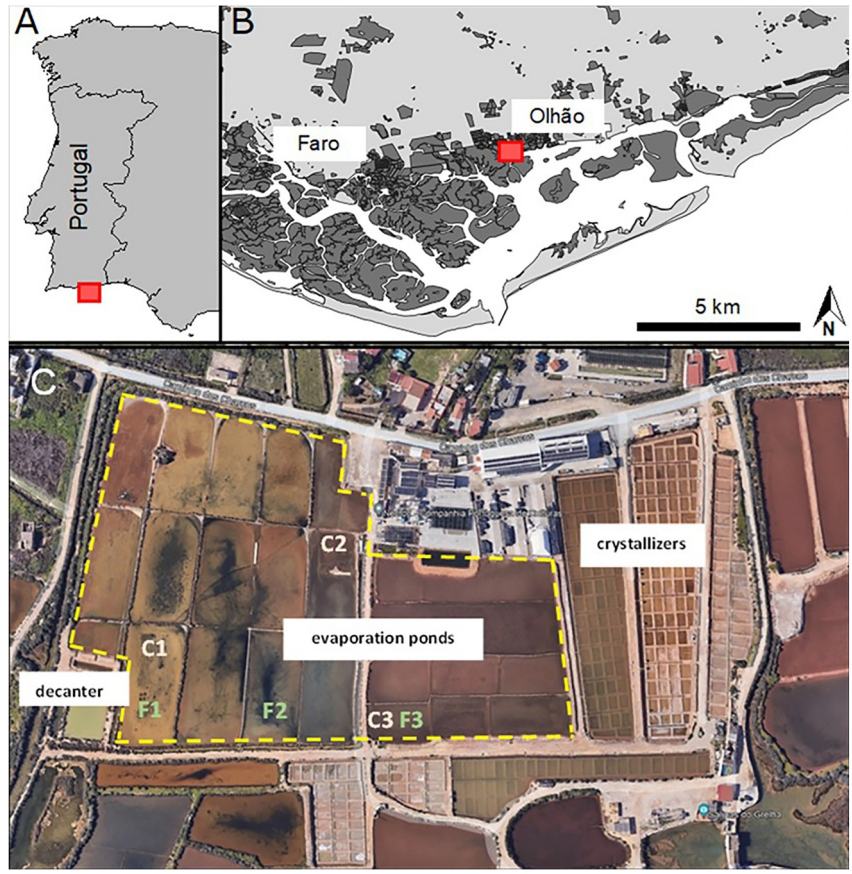

Figure 1. Location of the Ria Formosa lagoon in south Portugal (a), location of the salt ponds of Necton (Companhia Portuguesa de Culturas Marinhas, S.A.) within the lagoon (b), and aerial image of the salt ponds (c), showing the sites where the sediment cores were collected (C1, C2 and C3) and the sites where flux measurements were carried out (F1, F2 and F3). Site F2 was chosen over site C2 for the flux measurements because it was a better representative of the salinity gradient in the summer 2023, when the annual cycle was initiated. The evaporation ponds, indicated with a yellow dashed line, cover a total area of 42,500 m^2.

$$\text{Flux rate } (F) = (S \times V)/(R \times T \times A) \quad (1)$$

where F is the flux rate (μmol CH_4 or CO_2 m^{-2} h^{-1}), S (ppm s^{-1}) is the slope of the linear regression between the gas concentration (ppm) and time (s), V is the volume of the chamber and tubes (L), R is the ideal gas constant (L atm mol^{-1} K^{-1}), T is the air temperature inside the chamber (K), and A is the surface area of the chamber (m^2). Individual flux rates of CH_4 and CO_2 were time-integrated, converted to μmol m^{-2} and integrated over 24 hr (μmol m^{-2} d^{-1}).

2.3. Environmental Variables

At each site, the salinity and pH of the pond water were measured at the onset of the 24 hr cycle in the early morning, at solar noon and the next day before sunrise, except in autumn when the cycle was interrupted after 13 hr. Salinity (psu) was measured with a conductivity probe (VWR CO310) and pH was measured with a portable pH meter (Thermo Scientific™ Orion Star™ A221). Dissolved oxygen (mg L^{-1}) and water temperature (°C) were continuously measured at each site at 1-min intervals, using small self-contained optical sensors (miniDOT® logger, Precision Measurement Engineering; accuracy ±0.01 mg O_2 L^{-1} and ±0.1°C; in-house certified calibration). The air temperature inside the chamber was continuously recorded at 1-min intervals during incubation with a HOBO® temperature logger (ONSET). Wind speed (km h^{-1}) was recorded at 1-min intervals with a Watchdog 2,000 series station, positioned at a height of 5 m above the water surface of the ponds.

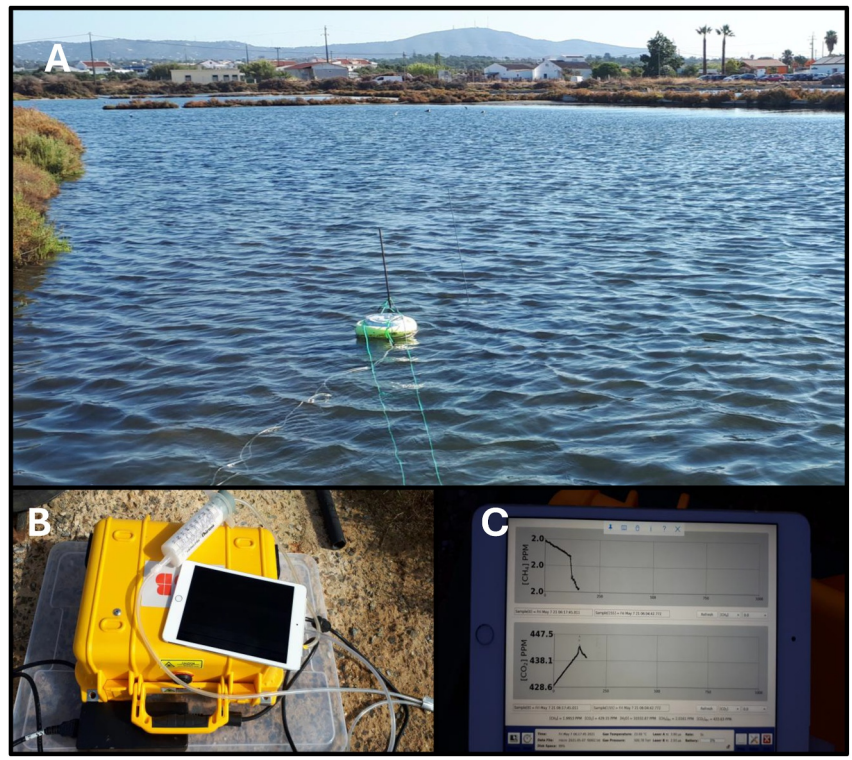

Figure 2. Measurement of water-air CH_4 and CO_2 fluxes: incubation chamber floating at the water surface (a), connected to the gas analyzer (b), which is paired with an iPad containing the software that allows real-time readings of the evolution of the gas concentrations inside the chamber (c).

2.4. Carbon Stocks

Sediment cores were taken in February 2021 at three sites (C1 to C3; Figure 1c). Cores (n = 3 per site) were extracted at each site by manually hammering 50-cm PVC tubes (internal diameter = 4.6 cm, bottom edge serrated) into the ground, until penetration was not further possible (penetration depth ranged from 32 to 42 cm; Table S1 in Supporting Information S1). Sediment cores were manually extracted in a vertical position by creating a vacuum using a stopper placed in the upper end of the tube. Immediately after extraction, the lower end of the tube was sealed with a lid to prevent sediment loss. Sediment compaction during coring was considered linear and was measured based on the total length of the corer, the empty space inside the cores with the sediment sample before retrieval, and the length of the sediment core retrieved, and ranged from 9.1% to 38.9% (Table S1 in Supporting Information S1). After extraction, the cores were sealed at both ends and transported to the laboratory in a vertical position, where they were immediately frozen at −20°C until further analysis.

At the laboratory, the sediment cores were opened lengthwise with a circular saw and the sediment profile was visually inspected to define the top OM-rich layer according to color and grain size (Figure S2 in Supporting Information S1). The sediment core from one half was divided into 1-cm slices and placed into pre-weighted zip-lock plastic bags, frozen at −20°C, oven dried (48 hr, 60°C), and weighed (dry weight, dw, ±0.001). The volume of the samples (cm^3) was estimated by geometrical approximation, using the thickness of each sample and the core diameter. Sediment dry bulk density (DBD, g dw cm^{-3}) was calculated as the dry weight divided by the volume of each sample. Dried samples were then manually ground to fine powder with a ceramic mortar and pestle. Fractions of 2–3 g dw from all samples (n = 263) were subjected to the loss-on-ignition procedure (LOI, 4 hr, 450°C) to estimate the OM content (OM, % dw). Organic Carbon content (OC, % dw) was determined in a selection of samples (n = 43, 16.3% of the total; Figure S3 in Supporting Information S1) by measuring the carbon content in the selected samples before and after LOI, using an automated elemental analyzer (Elementar, Vario EL III, Central of Technologies and Services, CCMAR). We observed that the OM content presented very high values (OM ≥ 12.5% dw) in many samples from site C3, which did not correspond to high OC content values (Figure S4 in Supporting Information S1). To verify analytical reliability, a subset of samples from site C3 was re-

analyzed for OM content using the LOI method, and elemental (CHN) analyses were repeated in an independent external laboratory; yet replicated measurements yielded consistent results. Therefore, these OM values were excluded from the analysis due to the suspicion of contamination with salts that might have interfered with the LOI procedure. To account for these missing values, we increased the number of samples for OC determination by elemental analyzer in cores from site C3 over the whole core depth and used only OC values to calculate the OC stocks in this pond (Figure S3 in Supporting Information S1). From the samples with valid OM and OC contents, a linear relationship was obtained to estimate OC values from sites C1 and C2: OC (% dw) = −0.862 + 0.307 OM (% dw) ($F_{1,20} = 46.2$, $p < 0.001$, adjusted $R^2 = 0.683$; Figure S4 in Supporting Information S1). When the linear regression yielded a negative value of OC, it was considered zero.

The sedimentary stock of OC per unit of area (g OC cm^{-2}) was estimated by multiplying OC content (g OC g^{-1} dw) by DBD (g dw cm^{-3}) for each depth interval, integrating these products over the depth of the core following standard techniques (Howard et al., 2014), and finally expressing the results in Mg OC ha^{-1}. Since the cores presented different penetration depths and compaction (Table S1 in Supporting Information S1), the compaction correction factor was calculated for each core to correct sediment depth. After applying this correction, depth of analysis for OC stocks was standardized to 30-cm, ensuring comparability among cores across sites.

2.5. Carbon Sequestration Rates

The sediment accumulation rate (mm yr^{-1}) was estimated by dividing the thickness of the OM-rich layer of each core by the number of years elapsed since the construction or major reconfiguration of the salt pond sites, hereafter referred to as the OM accumulation period. This approach assumes that the present OM-rich layer formed predominantly after the onset of the salt pond activity or its major reconfiguration, as these construction phases involved extensive sediment removal and reshaping, which likely removed or disturbed pre-existing surface sediments and promoted remineralization of previously deposited OM. The OM accumulation period was assessed using available aerial photographs of the site (Figure S1 in Supporting Information S1). The earliest available image dates to 1947, when the salt ponds already existed. A major reconfiguration occurred in 1972, during which the ponds at sites C1 and C2 were extensively modified, whereas site C3 remained largely unchanged. Based on this historical information, we estimated an accumulation period of 49 years for C1 and C2 (since 1972), and a minimum accumulation period of 74 years for site C3 (since 1947). Therefore, these estimates represent conservative approximations of post-construction sediment and OM accumulation.

The carbon sequestration rate (g OC m^{-2} yr^{-1}) was then obtained as the product of the sediment accumulation rate (mm yr^{-1}) of each core and the weighted average of the OC density (g OC cm^{-3}) considering only the depth corresponding to an age of 49 years (i.e., from the last major reconfiguration of the salt ponds, in 1972). The total OC stock (Mg OC) and the annual OC sequestration rate (Mg OC yr^{-1}) for the whole salt pond area were estimated as the product of the mean OC stock and mean OC burial rate per unit of area from the three sites and the total area covered by the evaporation ponds.

2.6. Flux Rates

Flux rates of CH_4 and CO_2 (F, μmol m^{-2} h^{-1}) measured along the diel cycles were integrated to obtain daily CH_4 or CO_2 flux rates (DFR_{CH4} or DFR_{CO2}; μmol m^{-2} d^{-1}) for each site and sampling period, applying the trapezoidal rule (Equation 2). For the diel cycle that did not extend to a full 24-hr period, the last measured flux rate was assumed constant to complete the integration over the remaining hours of the day.

$$\text{Daily flux rate (DFR)} = \sum_{i=1}^{n-1} \frac{(t_{i+1} - t_i) \times (F_{i+1} + F_i)}{2} + \left(24 - \sum_{i=1}^{n} t_i\right) \times F_n \quad (2)$$

where, i denotes each individual measurement taken during the sampling cycle, n represents the total number of flux measurements within the cycle, t corresponds to the time points at which the measurements were recorded (h), and F is the flux rate of CH_4 or CO_2 measured at each time point (μmol m^{-2} h^{-1}), as calculated using Equation 1.

Table 1
Summary of the Statistical Tests and Post hoc Comparisons Performed to Detect Significant Differences in the Specified Variables Among the Three Sites (Salt Ponds)

Variable	Season	Test used	Post hoc comparisons
CH_4	Spring, Summer, Autumn, Winter	Kruskal-Wallis	Dunn's test
CO_2	Summer	ANOVA	Holm Sidak
CO_2	Autumn/Winter/Spring	Kruskal-Wallis	Dunn's test
Salinity	Spring, Summer, Autumn, Winter	ANOVA	Holm Sidak
pH	Spring, Summer, Autumn, Winter	ANOVA	Holm Sidak
O_2	Summer, Autumn, Winter	Kruskal-Wallis	Dunn's test
O_2	Spring	ANOVA	Holm Sidak
Water temperature	Spring, Summer	Kruskal-Wallis	N/A
Water temperature	Autumn, Winter	ANOVA	N/A
Wind speed	Summer	ANOVA	N/A
Wind speed	Autumn, Winter, Spring	Kruskal-Wallis	N/A

The daily CO_2 and CH_4 flux rates were expressed as CO_2 equivalents (CO_2-eq) and summed to calculate the total flux rates (DFR_{Total}, μmol CO_2-eq m^{-2} d^{-1}). CH_4 fluxes were converted to CO_2-eq by applying a factor of 28, representing the 100-year global warming potential of CH_4 as defined by the IPCC (2021).

Seasonal flux rates of CH_4 and CO_2 (SFR_{CH4} or SFR_{CO2}; mmol m^{-2} $season^{-1}$) were calculated by multiplying the daily flux rates of CO_2 or CH_4 by the number of days in the respective season and converting the results to mmol. The total seasonal flux rate (SFR_{Total}; mmol CO_2-eq m^{-2} $season^{-1}$) was then obtained by summing the seasonal flux rates of CH_4 and CO_2 after converting CH_4 fluxes into CO_2-eq by applying a factor of 28 (IPCC, 2021). Finally, the four seasonal total flux rates were summed to calculate the total annual flux rate (AFR_{Total}; mmol CO_2-eq m^{-2} yr^{-1}) for each site.

2.7. Annual Carbon Budget

A simple carbon budget model (Equation 3) was developed for the whole salt pond evaporation area to estimate the annual net carbon flux rate (NCF; g CO_2-eq m^{-2} yr^{-1}). A positive value of NCF indicates that the salt pond is a carbon sink, whereas a negative value indicates that it is a carbon source. The limitations of this simple model will be assessed in the Discussion section.

$$\text{Annual Net Carbon Flux Rate (NCF)} = \text{AFR} + \text{SR} \quad (3)$$

where AFR is the annual total carbon flux rate and SR is the OC sequestration rate in the sediment, both expressed in g CO_2-eq m^{-2} yr^{-1}. The SR, initially expressed in g OC, was converted to CO_2-equivalents by multiplying by 3.67, the mass ratio of CO_2 to carbon. The AFR, initially expressed in mol CO_2-eq, was expressed in g CO_2-eq by multiplying its value by 44.01 g mol^{-1}, the molecular weight of CO_2.

2.8. Statistical Analysis

The slopes S used in the calculation of CH_4 and CO_2 flux rates were obtained using least squares linear regression. Table 1 summarizes the statistical tests used to detect significant differences in the flux rates of CH_4 and CO_2, as well as in the environmental parameters among the three salt ponds studied.

ANOVA results were reported with the F value, while Kruskal-Wallis results were reported with χ^2, with the respective degrees of freedom (d.f.) and the associated p-value. Differences were considered significant at a level of $p < 0.05$. Statistical analyses were performed using SigmaPlot V14.

Two multiple linear regressions at $p > 0.05$ (IBM SPSS Statistics 21) were performed separately to identify predictors of CH_4 and CO_2 fluxes because of the different number of observations of the predictor variables. One

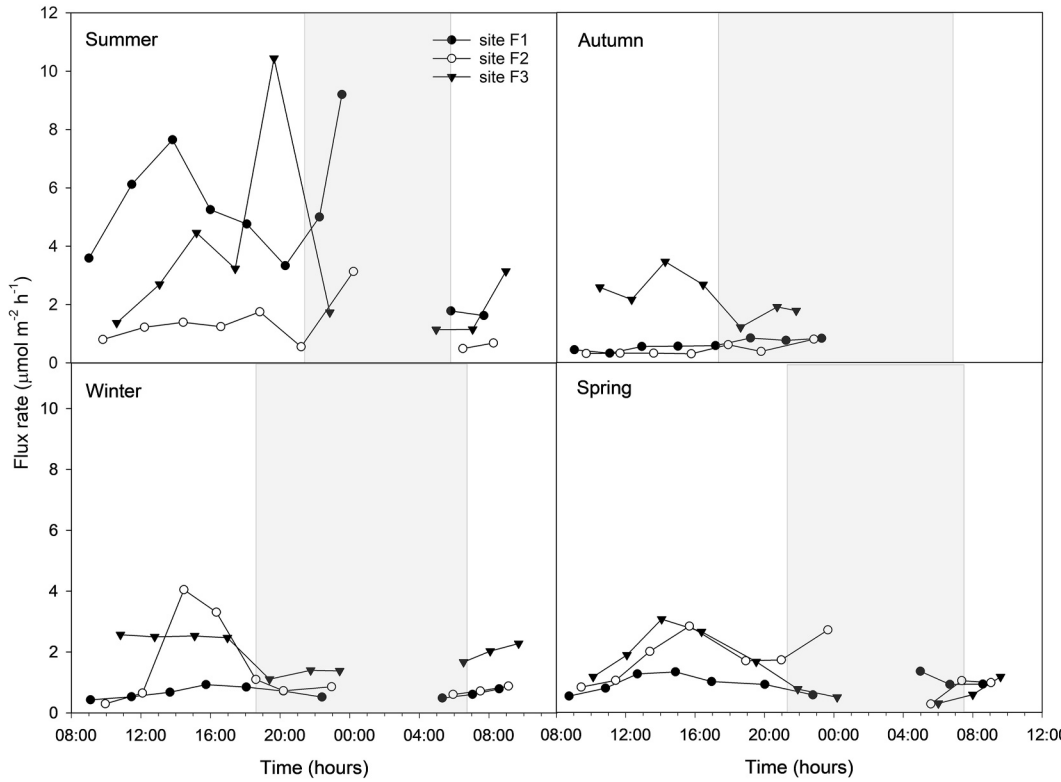

Figure 3. Diel variation in the CH_4 flux rates across the three sites (F1, F2 and F3) over the four seasons. Gray shaded areas represent the night-time period.

multiple linear regression was performed with salinity and pH, each with $n = 33$ observations, and another multiple linear regression with water temperature, oxygen and wind, each with $n = 110$ observations.

Sedimentary OC content in the top 30-cm did not meet parametric assumptions even with data transformation, so non-parametric Kruskal-Wallis rank sum tests were used to test for differences among sites (fixed factor, three levels: sites C1, C2 and C3), followed by post hoc Dunn's test, with Bonferroni correction, to assess pairwise differences among them. Differences in the upper 30-cm OC stocks and sequestration rates among sites were tested with one-way ANOVA and Tukey post hoc tests, which control the family-wise error rate of multiple comparisons, after testing normality (Shapiro-Wilk test) and homoscedasticity (Flinger test) of the data. A significance level of 0.05 was considered for all tests. Statistical analyses for sedimentary carbon data were performed in the R programming language (version 4.3.1; R Core Team, 2023) and RStudio software (version 2023.06.1). The data set generated in this study is available in Zenodo (de los Santos & Alexandre, 2026, https://doi.org/10.5281/zenodo.17867948).

3. Results

3.1. CH_4 and CO_2 Fluxes

The three sites (F1 to F3) emitted CH_4 to the atmosphere throughout the year, with no consistent daily pattern along sites or seasons (Figure 3). In the summer, emission rates at sites F1 and F3 were significantly higher ($H = 13.70$, d.f. $= 2$, $p < 0.001$) than at site F2 (Table 2). In autumn, CH_4 emission rates at site F3 were significantly higher ($H = 15.16$, d.f. $= 2$, $p < 0.001$) than at F1 and F2, which were similar (Table 2). In winter, despite the peak of CH_4 emission in site F2 during the day (Figure 3), the mean flux was similar to sites F1 and F3, which differ significantly ($H = 14.87$, d.f. $= 2$, $p < 0.001$). In spring, CH_4 fluxes were not significantly different among sites ($H = 2.33$, d.f. $= 2$, $p = 0.321$) (Figure 3, Table 2).

Similar to CH_4, there was no clear daily pattern of CO_2 fluxes along sites or seasons (Figure 4). Most sites absorbed CO_2 throughout the year except in Spring when water to air emissions were high, particularly of site F2

Table 2
Weighted Average (± Weighted Standard Deviation) of CH_4 and CO_2 Flux Rates (μmol m^{-2} h^{-1}) Over Each Sampling Cycle, Daily CH_4 and CO_2 Flux Rates (mmol m^{-2} d^{-1}), Daily Total Flux Rate (mmol CO_2-Eq m^{-2} d^{-1}) and Seasonal CO_2-Eq Flux Rate (mmol m^{-2} $Season^{-1}$)

Season	Site	Average CH_4 flux (μmol m^{-2} h^{-1})	Average CO_2 flux (μmol m^{-2} h^{-1})	Daily CH_4 flux (mmol m^{-2} d^{-1})	Daily CO_2 flux (mmol m^{-2} d^{-1})	Daily total CO_2-eq flux (mmol m^{-2} d^{-1})	Seasonal CO_2-eq flux (mmol m^{-2} $season^{-1}$)
Summer	F1	5.7 ± 2.6 (n = 10)	−278.3 ± 234.9 (n = 10)	0.119	−6.650	−3.322	−305.6
	F2	1.6 ± 1.0 (n = 9)	−423.8 ± 152.3 (n = 9)	0.033	−9.710	−8.777	−807.5
	F3	3.3 ± 3.0 (n = 9)	318.2 ± 145.6 (n = 9)	0.076	7.317	9.454	869.8
Autumn	F1	0.7 ± 0.2 (n = 8)	−67.8 ± 35.4 (n = 8)	0.017	−1.610	−1.140	−103.8
	F2	0.6 ± 0.2 (n = 7)	−299.5 ± 75.6 (n = 7)	0.014	−7.424	−7.023	−639.1
	F3	2.1 ± 0.6 (n = 7)	−187.2 ± 37.0 (n = 7)	0.049	−4.610	−3.249	−295.6
Winter	F1	0.6 ± 0.2 (n = 10)	−312.9 ± 97.5 (n = 10)	0.015	−7.599	−7.175	−645.7
	F2	1.3 ± 1.1 (n = 10)	−336.3 ± 113.6 (n = 10)	0.030	−7.784	−6.932	−623.9
	F3	1.9 ± 0.6 (n = 10)	−33.8 ± 57.6 (n = 10)	0.045	−0.860	0.395	35.6
Spring	F1	0.9 ± 0.3 (n = 10)	238.2 ± 84.2 (n = 10)	0.024	5.747	6.431	591.7
	F2	1.9 ± 0.9 (n = 10)	813.5 ± 255.3 (n = 10)	0.041	18.479	19.629	1,805.9
	F3	1.4 ± 1.0 (n = 10)	192.7 ± 61.1 (n = 10)	0.032	4,458	5,359	493.0

(Figure 5, Table 2). Site F3 was a significant source of CO_2 in the Summer, as opposed to sites F1 and F2 (F = 33.80, d.f = 2, p < 0001) which had similar negative fluxes. In autumn, the CO_2 uptake in site F2 was significantly higher than site F1 (H = 13.85, d.f. = 2, p < 0.001). In winter, the CO_2 uptake of site F3 was significantly lower (H = 19.56, d.f. = 2, p < 0.001) than sites F2 and F1. In spring, the emission rate of site F2

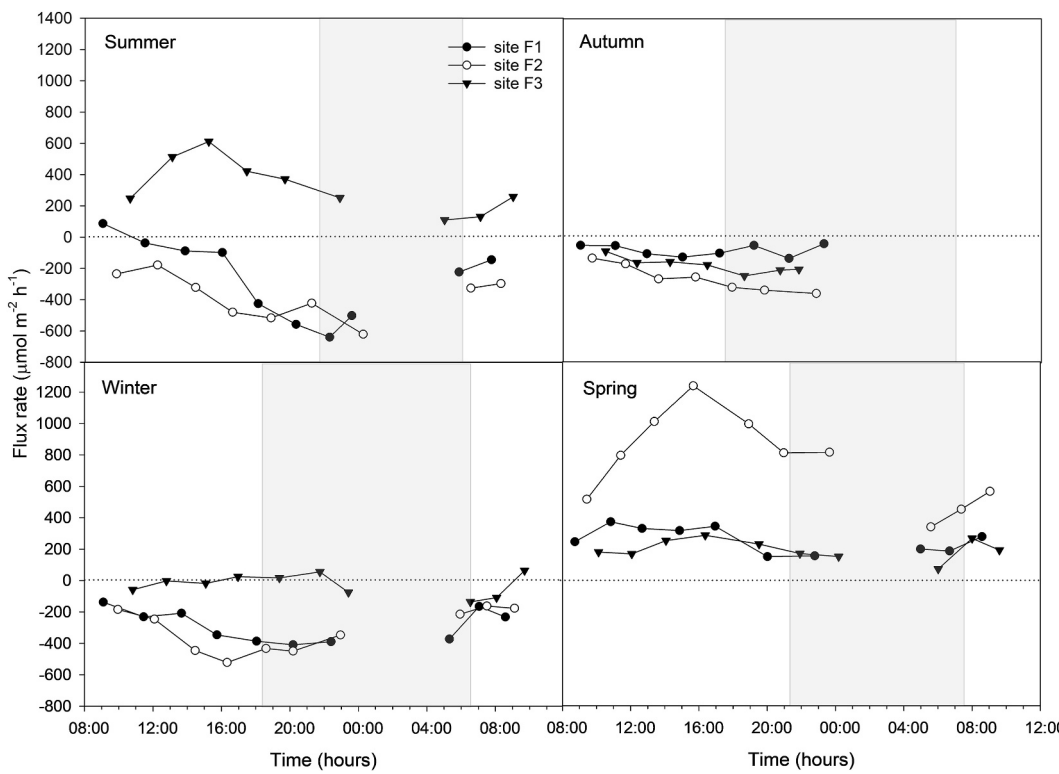

Figure 4. Diel variation in the CO_2 flux rates across the three sites (F1, F2 and F3) over the four seasons. Gray shaded areas represent the night-time period.

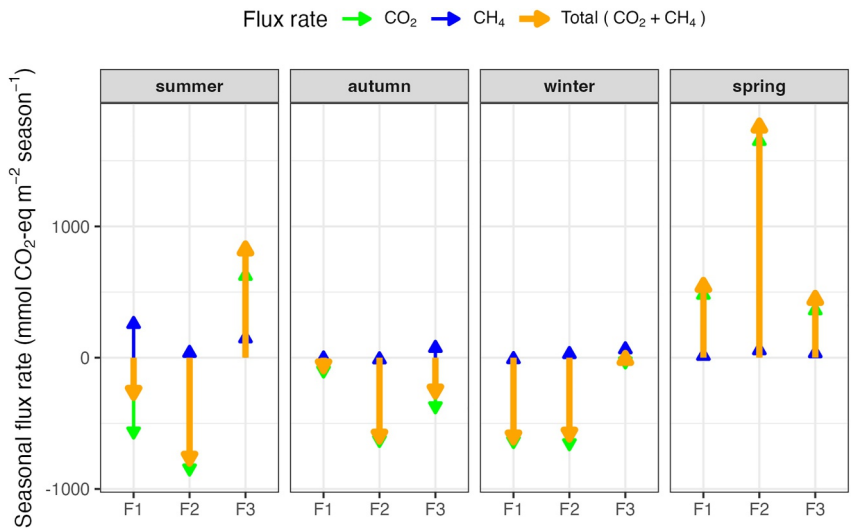

Figure 5. Seasonal flux rates (expressed in CO_2-eq) originated from CH_4 and CO_2, and total flux rate (sum of both rates) across sites (F1, F2, and F3). Downward arrows indicate that the flux was from the atmosphere to the water (carbon sink), while upward arrows indicate the opposite direction (carbon source).

was significantly higher (H = 19.73, d.f. = 2, $p < 0.001$) than sites F1 and F3. Blooms of *Artemia salina* were observed at sites F2 in spring and F3 in summer, coincident with peaks in CO_2 emissions (Figures 4 and 5, Table 2).

The net CO_2-eq fluxes followed the pattern of the CO_2 fluxes, showing that the pond system was a sink of CO_2 in all seasons, except in spring and site F3 in summer (Figure 5, Table 2). The highest fluxes were found at site F2 in the summer. On average, the saltern was a source of CO_2-eq in spring (963.5 mmol m^{-2} $season^{-1}$), and a sink of CO_2-eq in summer (−81.1 mmol m^{-2} $season^{-1}$), autumn (−346.2 mmol m^{-2} $season^{-1}$) and winter (−411.3 mmol m^{-2} $season^{-1}$). Preliminary flux measurements carried out in 2021 confirmed that the system was a CO_2-eq sink in winter and a source in spring, with persistent CH_4 emissions on both seasons (Figure S5 in Supporting Information S1).

3.2. Environmental Drivers of CH_4 and CO_2 Fluxes

The environmental variability among sites and across seasons is presented in (Figures S6–S10 in Supporting Information S1). Multiple linear regressions identified water temperature as the main, positively related predictor variable of CH_4 fluxes (Table 3). On the other hand, CO_2 fluxes were significantly negatively related to the concentration of O_2 and pH in the seawater and positively related to wind (Table 3). The percentage of variance of CH_4 fluxes explained by environmental variables is low (<0.30%, Table 3) as opposed to CO_2 fluxes (0.66%, Table 3).

3.3. Organic Carbon Profiles, Stocks, and Sequestration Rates

The variation of OC contents with depth followed a general decreasing pattern at all sites, with site C3 presenting higher values (Figure 6). The mean OC contents at the top 30-cm sediment layer were significantly different among sites ($\chi^2 = 55$, d.f. = 2, $p < 0.05$), with C1 (0.99 ± 0.12% dw, $n = 56$) and C3 (2.58 ± 0.19% dw, $n = 771$) showing higher OC contents than C2 (0.33 ± 0.07% dw, $n = 68$).

Sedimentary OC stocks presented high within-site variability within each site, especially in C2, while no significant differences were observed among sites (Table 4), with an overall mean of 11.9 ± 2.2 Mg OC ha^{-1}. Mean sediment accumulation rates varied 2.4-fold across sites, being significantly lower at C2 than at C1 and C3 (Table 4). Mean OC burial rates since the last major reconfiguration of the salt ponds in 1972 were similar among sites, ranging between 6.3 and 14.6 g OC m^{-2} yr^{-1} (Table 4), with a mean value of 11.1 ± 4.3 g OC m^{-2} yr^{-1}. The estimated total OC stock in the top 30-cm layer of the sediment for the evaporation pond area was 50.6 Mg OC, and the annual OC burial rate was 0.472 Mg OC yr^{-1}.

Table 3
Results of the Multiple Linear Regressions of Predictor Variables on the CH_4 and CO_2 Fluxes Using the Daily Average Values of Each Predictor Variable and Gas Flux Obtained for the Three Sites Across the Four Seasons

	CH_4 flux		CO_2 flux	
	β	p-value	β	p-value
Salinity	−0.229	0.654	−0.099	0.739
pH	−0.256	0.617	**−0.906**	**0.005**
Model	$R^2 = 0.009$, $p = 0.880$, $n = 33$		$R^2 = 0.663$, $p < 0.001$, $n = 33$	
Water temperature	**0.500**	**<0.001**	−0.080	0.774
Water oxygen	0.053	0.529	**−0.364**	**<0.001**
Wind	0.053	0.568	**0.621**	**<0.001**
Model	$R^2 = 0.293$, $p < 0.001$, $n = 110$		$R^2 = 0.413$, $p < 0.001$, $n = 110$	

Note. Bold values are significant at $p < 0.05$. β = standardized regression coefficients.

3.4. Annual Carbon Budget

Net CO_2 uptake rates of −20.4 g CO_2-eq m^{-2} yr^{-1} and -11.6 g CO_2-eq m^{-2} yr^{-1} were estimated for sites F1 and F2, and a net CO_2 emission rate of 48.5 g CO_2-eq m^{-2} yr^{-1} for site F3, which corresponds to an average emission rate of CO_2 of 5.5 ± 37.5 g CO_2-eq m^{-2} yr^{-1} (Table 5, Figure 7). The average OC burial rate of the saltern was 11.0 ± 4.3 g OC m^{-2} y^{-1}, which corresponds to a carbon sequestration rate by the sediments of 40.5 ± 15.6 g CO_2-eq m^{-2} yr^{-1} (Figure 7). This value is, on average, nearly 7-fold higher than the estimated CO_2 emission rate, rendering the saltern a net sink of CO_2. For the entire evaporation pond area, the estimated carbon emission rate was 0.23 ± 1.60 Mg CO_2-eq yr^{-1}, while the carbon burial rate was −1.72 ± 0.66 Mg CO_2-eq yr^{-1}, resulting in a net carbon budget of −1.49 ± 1.27 Mg CO_2-eq yr^{-1} (Figure 6).

Assuming that the blooms of *Artemia sp.* do not last more than 1 month (Baxevanis et al., 2004; Browne et al., 1988), we calculated the daily fluxes of F3 in summer and daily fluxes of F2 in spring as the average of the other two ponds, where blooms of *Artemia* sp. did not occur. The fluxes estimated for F3 and F2 were −67.3 and −14.2 g CO_2-eq m^{-2} yr^{-1}, respectively. Recalculating for the whole evaporation pond area, the estimated carbon uptake rate is −1.44 ± 1.23 Mg CO_2-eq yr^{-1}, which means that the net annual carbon budget of the whole pond system lies between −1.49 and −3.16 Mg CO_2-eq yr^{-1}, rendering the whole system a relevant carbon sink.

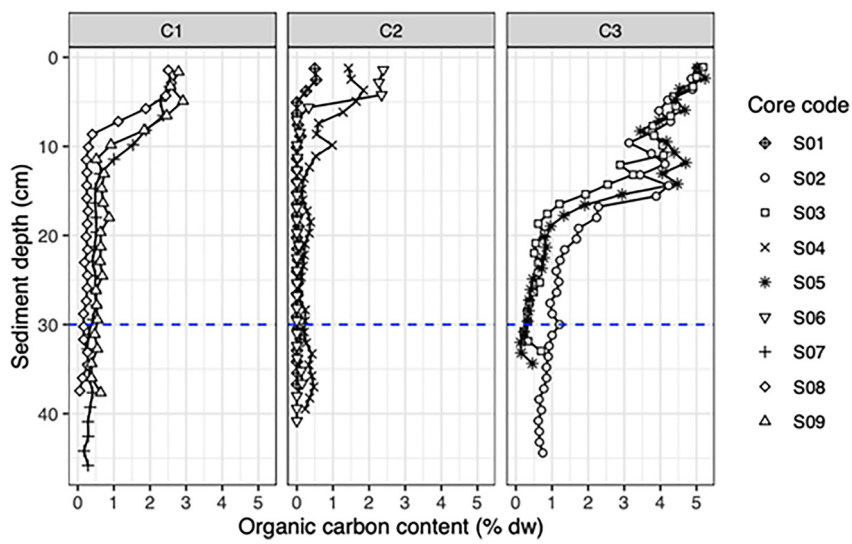

Figure 6. Sediment profile of Organic Carbon (OC) content at sites C1,C2 and C3 (see Figure 1 for site location). The blue dashed line represents the depth used to estimate the OC stock.

Table 4
Sedimentary Organic Carbon (OC) Stocks (Top 30-cm Layer), Sediment Accumulation Rates, Estimated Based on Reconstruction Analysis, and OC Burial Rates Since the Last Major Reconfiguration of the Evaporation Ponds in 1972

	C1	C2	C3	Statistics
OC stock (Mg OC ha^{-1})	12.6 ± 1.9 (9.1–15.5)	6.3 ± 4.0 (1.9–14.3)	16.9 ± 2.9 (11.8–21.7)	$F_{2,6} = 3.1$, $p > 0.05$
SAR (mm yr^{-1})	2.4 ± 0.2[a] (2.1–2.8)	0.9 ± 0.2[b] (0.5–1.3)	2.5 ± 0.1[a] (2.4–2.6)	$F_{2,6} = 18.4$, $p < 0.01$
OC burial rate (g OC m^{-2} yr^{-1})	12.2 ± 1.5 (9.4–14.6)	6.3 ± 2.7 (3.3–11.9)	14.6 ± 2.3 (10.6–18.7)	$F_{2,6} = 3.4$, $p > 0.05$

Note. Values are mean ± SE ($n = 3$), with maximum and minimum values given in parentheses. Different superscript letters indicate significant differences among sites (Tukey HSD).

4. Discussion

Our study showed that the traditional saltern under study was a source of CH_4 in all seasons, whereas it was a sink of CO_2 in summer, autumn and winter, and a source in spring. By integrating the discrete measurements of the air-water carbon fluxes with the sediment burial rates, we estimated that the annual carbon sink was between −1.49 and −3.16 Mg CO_2-eq yr^{-1}, rendering the whole salt pond area a significant carbon sink.

The air-water CH_4 fluxes were within, but close to the lower end of the range of air-water fluxes measured in coastal ecosystems elsewhere (Table 6). In general, the CH_4 emissions of saltmarshes, the natural ecosystem replaced by salt ponds, are higher. This may be due to differences in salinity, which is negatively correlated with CH_4 production in coastal wetlands (Al-Haj & Fulweiler, 2020; Poffenbarger et al., 2011). Competition for substrates (acetate and H_2) between sulfate-reducing bacteria and acetoclastic and hydrogenotrophic methanogens may occur in salty environments, with sulfate reducers outcompeting methanogens given their higher affinity for competitive substrates and limiting CH_4 production (Keneally et al., 2024), although sulfate reduction and methanogenesis may co-occur in sediment with high OC loading (Holmer & Kristensen, 1994). In addition, high salinity induces osmotic stress on microbial metabolism, therefore requiring methanogens to produce or consume compatible solutes to balance osmotic pressure, an energetically expensive process that can result in reduced CH_4 production (McGenity & Sorokin, 2019). On a global scale, CH_4 emissions in seagrass meadows were within those of salt marshes, although no correlation has been found between salinity and CH_4 fluxes in seagrass ecosystems (Al-Haj & Fulweiler, 2020). With respect to CO_2, the saltmarshes of the nearby Bay of Cadiz behave as sources, whereas the saltern studied in Ria Formosa is a net sink, with values within the range of those reported for mixed-vegetation communities of vascular plants and algae in the Baltic Sea (Table 6).

CO_2 fluxes fluctuated without a clear pattern along the diel cycle, while CH_4 emission rates were about 30% higher during the day than at night. This highlights the importance of measuring fluxes over full diel cycles, as point measurements during daytime or night-time may provide biased estimates of the fluxes. Even though diel variability in the fluxes of both gases has been observed in a range of ecosystems, there is a lack of consensus in the reported results. Some studies reported maximum emissions of CH_4 during the night in seagrass meadows (Bahlmann et al., 2015), salt marshes (Diefenderfer et al., 2018) and restored bogs (Dooling et al., 2018). Others report maximum emissions during the day in mangroves and salt marshes (Yang et al., 2018), mixed-vegetation

Table 5
Annual CH_4, CO_2, and Total (CH_4 + CO_2) Fluxes in the Evaporation Area of the Saltern

Site	Annual CH_4 flux rate (mmol CH_4 m^{-2} yr^{-1})	Annual CO_2 flux rate (mmol CO_2 m^{-2} yr^{-1})	Annual total flux rate (mmol CO_2-eq m^{-2} yr^{-1})	Annual total flux rate (g CO_2-eq m^{-2} yr^{-1})
F1	16.1	−913	−463	−20.4
F2	10.9	−569	−265	−11.6
F3	18.4	586	1,103	48.5
All	15.1 ± 3.9	−298 ± 785	124 ± 852	5.5 ± 37.5

Note. The average ± SD for the three sites is also shown.

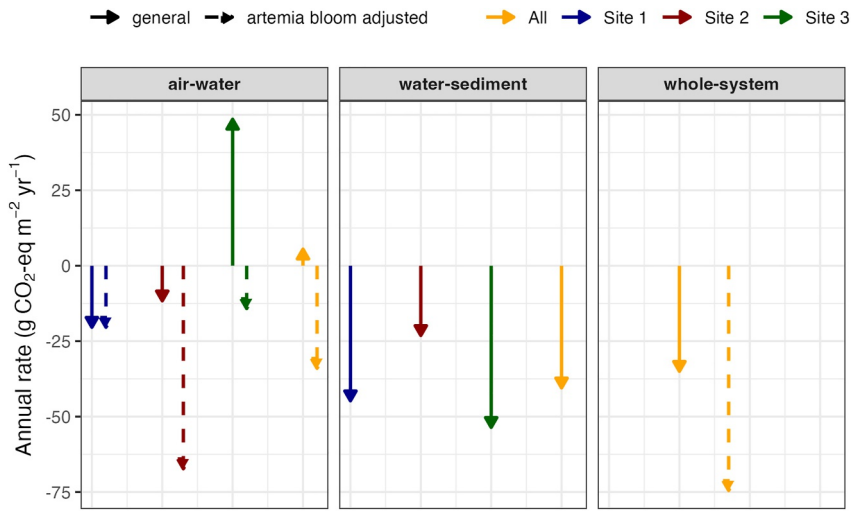

Figure 7. Annual carbon flux rates at the air-water and water-sediment interfaces, and the sum of both interfaces (whole-system). Downward arrows indicate that the flux was from the atmosphere to the water or from water to the sediment (carbon sink), while upward arrows indicate the opposite direction (carbon source). The "All" arrow depicts the average of the three sites.

ecosystems (Roth et al., 2023), seagrass meadows (Yau et al., 2023) and lakes (Sieczko et al., 2020). This discrepancy is probably related to the different communities dominating each ecosystem. In the salt ponds, CO_2 uptake rates were higher during the day as a natural result of photosynthesis. Curiously, during the night the system continued absorbing CO_2. We speculate that this may be a combination of factors. On one hand, the dark uptake of CO_2 by tropical saltmarshes has been documented by Iram et al. (2021), suggesting the presence of carbon fixation pathways independent of light in coastal systems. Chemosynthetic microbes such as acetogens that are abundant in the anoxic sediments of wetlands and fixate CO_2 in the dark, may provide a relevant carbon sink pathway (Rodriguez et al., 2025). On the other hand, there is the possibility that lower concentrations of CO_2 in the water column than in the air resulting from photosynthesis during the day persisted and were not reverted during the night period by respiration. Unfortunately, the alkalinity measurements we performed to assess the CO_2 concentration in the water were not reliable, probably due to the high levels of salinity.

The CO_2 source to sink shifts observed in site F2 in spring, and in site F3 in summer, may be related to higher respiration caused by the blooms of *Artemia salina* that were observed in those sites. The same shifts were

Table 6
Summary of the Ranges of CH_4 and CO_2 Fluxes Reported in Different Coastal Ecosystems

Flux rate (μmol m^{-2} d^{-1})		Ecosystem	Location	Source
CH_4	4.4 to 41.4	Salt ponds converted into wetlands	California, USA	Zhou et al. (2021)
CH_4	34 to 150	Salt marshes	Cadiz, Spain	Ferrón et al. (2007)
CH_4	2.6 to 720	Salt marshes	Doñana, Spain	Huertas et al. (2019)
CH_4	−93 to 94,000	Salt marshes	global scale	Al-Haj and Fulweiler (2020)
CH_4	1.3 to 402	Seagrasses	global scale	Al-Haj and Fulweiler (2020)
CH_4	0.45 to 4.5	Seagrasses	Baltic Sea	Asplund et al. (2022)
CH_4	0.12	Seagrasses	Mediterranean Sea	Yau et al. (2023)
CH_4	6.25 to 181.25	Mixed-vegetation communities	Baltic Sea	Roth et al. (2023)
CH_4	14 to 119	Salterns	Portugal	This study
CO_2	−17336 to 8,861	Mixed-vegetation communities	Baltic Sea	Roth et al. (2023)
CO_2	7,300 to 177,000	Salt marshes	Cadiz, Spain	Ferrón et al. (2007)
CO_2	−860 to 18,479	Salterns	Portugal	This study

observed in sites F1 and F3 in spring (but not in sites F1 and F2 in summer), indicating that secondary production in spring may be the underlying cause. Nevertheless, other causes may contribute to these shifts observed when the temperature was higher and salinity doubled. A greater abundance of sulfate reducers is expected with increased salinity (Al-Haj & Fulweiler, 2020), and consequently, a greater release of CO_2 due to increased microbial respiration. It is also possible that the increase in ionic strength associated with increased salinity results in a greater carbon availability through the desorption of previously protected labile OM from soil surfaces (Neubauer et al., 2013), with a consequent higher CO_2 release.

The negative correlation of CO_2 fluxes with pH and oxygen suggests that these fluxes were mainly controlled by the biological metabolism of the ponds. A shift from autotrophic to heterotrophic conditions within the ponds will reduce the oxygen concentration. On the other hand, the CO_2. Released by the respiratory activity forms carbonic acid that dissociates and releases hydrogen ions, lowering the seawater pH (Schulz et al., 2023). Wind has a positive effect on pond CO_2 uptake as it increases the gas transfer velocity through the increase of surface turbulence that increases the surface area and disrupts the boundary layer reducing resistance to gas diffusion (Jähne, 2019; Wanninkhof & Triñanes, 2017). In fact, in spring and summer, when CO_2 effluxes were higher, wind speed was also 6 to 12-fold higher relative to autumn and winter, reaching maximum speeds of 15 and 25 km hr^{-1}. In a shallow-water pond in China, winds of 12 km hr^{-1} increased CH_4 and CO_2 effluxes by 6 and 160-fold, respectively, relative to weaker wind conditions (Zhang et al., 2023). CO_2 fluxes were also primarily influenced and amplified by small-scale winds (up to 18 km hr^{-1}) in a tropical coastal sea in Malaysia (Yusup et al., 2023).

Higher CH_4 fluxes were associated with higher water temperature. Temperature has been recognized as an important driver for both CH_4 and CO_2 production and flux in a variety of environments across microbial to ecosystem scales (Yvon-Durocher et al., 2014), such as vegetated coastal systems (Al-Haj & Fulweiler, 2020; Ferrón et al., 2007; George et al., 2020; Huertas et al., 2019) and salt pans (Thomas et al., 2014), as increasing temperature increases microbial metabolism, including methanogenesis (Segers, 1998). This may explain the higher fluxes of CH_4 observed during the day relative to night-time, when pond water temperatures were about 8–10°C lower.

There are a limited number of studies that have measured sedimentary carbon in active salterns. Some studies measured sedimentary carbon in abandoned salt ponds or salt ponds reconverted from salt marshes and mangroves, but our results cannot be directly compared with them because not enough information was provided. The sediment depth used to determine the carbon content was not indicated (Ma et al., 2019; Yu et al., 2012), the stocks were calculated using a different depth (Gulliver et al., 2020), or stocks are reported as total carbon (Castillo et al., 2017). In our study, we reported a carbon content of 0.33%–2.58% and a density of 2.11–17.02 mg OC cm^{-3} for the top 30 cm among the three sites, within the same range that those reported by Gulliver et al. (2020) in saltponds, with a mean carbon content of 1.42 ± 0.09% and a carbon density of 13.7 ± 1.4 mg OC cm^{-3} for the top 20 cm. Nonetheless, the mean sedimentary carbon contents reported in both studies for abandoned salt ponds are higher than those measured in our study (<1%). It should be noted, however, that Castillo et al. (2017) reported total carbon, assuming that inorganic carbon in their sediment is negligible.

The carbon stock measured in the saltern, 12 Mg OC ha^{-1}, is within the lower end of the 95% confidence interval of those measured in the pioneer salt marsh of the adjacent Ria Formosa lagoon, re-calculated to a comparable depth, 17.2–30.4 Mg OC ha^{-1} (Martins et al., 2022). Larger differences were found between the sequestration rates of the salt ponds (6.3–14.6 g m^{-2} yr^{-1}) and the adjacent Ria Formosa saltmarsh, which ranged from 19.35 to 33.95 g m^{-2} yr^{-1} (Martins et al., 2022), suggesting that the replacement of salt marsh by salt ponds decreases the potential for carbon sequestration of the original ecosystem. The carbon stock measured in our study is substantially lower than the global average of 79.2 ± 38.1 Mg OC ha^{-1} for tidal marshes (Maxwell et al., 2023). We expect this difference to be even larger when looking at longer timescales, because the OC profiles show a very sharp decrease in OC content with depth. Additionally, the periodic maintenance of the salt ponds results in the removal of the sequestered OM and its exposure to oxygen, promoting re-mineralization. This idea is supported by Ramjattan (2022), who observed that modified salt marsh sediments tend to store less carbon overall, but with a more pronounced difference for deeper sampling depths.

There are very few studies that allow for a direct comparison between the air-water carbon fluxes (CO_2 and CH_4) and the water-sediment OC fluxes in blue carbon ecosystems, so that the overall carbon budget of the ecosystem

can be estimated. Weston et al. (2014) reported a net sink of carbon of 100–340 g CO_2-eq m^{-2} yr^{-1} in a mesohaline saltmarsh dominated by *Spartina alterniflora*, in the Delaware river, New Jersey, USA, integrating CO_2 and CH_4 exchange rates with the atmosphere, and the carbon burial in the sediment. The net annual carbon sink of 35 g CO_2-eq m^{-2} yr^{-1} measured in the saltern of Ria Formosa was about 10-fold lower.

At this point, it is important to acknowledge the errors associated with the CO_2 and CH_4 flux data measured in this work that should be considered with caution in the calculation of the annual carbon budget of Ria Formosa salt ponds. First, the night-time flux data for a period of 6–7 hr is missing in all seasons, with implications in the net flux estimates, particularly in autumn when no flux data is available for the night period. Even though care was taken in order to perform at least one flux incubation after sunset and before sunrise, that is in complete darkness, in order to capture the start and end point flux values during night-time, the occurrence of peak emissions of CO_2 originated from occasional bubble ebullition during the night period cannot be discarded. Such occasional CO_2 peak fluxes would add to the total daily CO_2 flux but would hardly alter the saltern's function as a carbon sink given its large carbon burial capacity. Second, and probably more importantly, the seasonal fluxes were calculated based on single 24 hr measurements within each season. This low sampling frequency certainly represents a large source of error, as evidenced by the important metabolic influence of the sporadic *Artemia* sp. blooms, as we assume no intra-seasonal variability. It does not account for short-term extreme events either, which may substantially influence CO_2 fluxes. It has been shown that heavy rainfall may increase CO_2 emissions by 200% in shallow ponds in response to a drop in the atmospheric pressure, with little effect on CH_4 fluxes (Zhang et al., 2024). On the other hand, heatwaves may stimulate microphytobenthos photosynthetic activity and increase the uptake of CO_2 (Douglas et al., 2025), although it may be inhibited above 35°C (Vieira et al., 2013). The temperature of the overlying water in the ponds during summer reached this temperature, potentially reducing the effectiveness of carbon uptake capacity of the saltern. Ideally, flux measurements should be taken on several days of contrasting weather throughout a season to capture rapid changes in flux dynamics driven by variable weather.

In this study, the carbon budget was calculated accounting only for the air-water CH_4 and CO_2 exchanges and the sedimentary OC burial. It may be argued that other potentially relevant contributions should be considered, including the import of dissolved inorganic carbon and dissolved and particulate OC from the adjacent lagoon system. However, man-made salterns are artificial habitats where the input of water from the adjacent lagoon ecosystem is very low, and mostly in late spring and summer to account for evaporation. Most of the OC buried in the saltern sediments originates from within pond production and lateral export of biomass from the saltmarsh plants that occupy the slopes that contain the ponds. This import of OM was not quantified. Further studies should focus on revealing the potential sources of buried carbon and the relevant pathways of carbon input and output in the saltern, either by using isotopic or biomarker analyses or eDNA.

The approach used here to estimate carbon burial rates, dividing the thickness of the OM-rich layer by the time since the pond was constructed, assumes that the variation of the sedimentation and OM accumulation rates along time is constant. This limits the ability to accurately determine sedimentation rates and temporal variability in carbon accumulation, as opposed to radiometric methods. However, methods such as the excess ^{210}Pb from atmospheric input equally assume that both sedimentation rate and ^{210}Pb flux are constant, which is rarely valid in natural systems. In addition, the ponds are regularly visited by long-legged avifauna, which may induce sediment mixing, potentially complicating the application and interpretation of ^{210}Pb dating method. We note that the OM-rich layer was clearly distinguishable in the sediment profile, supporting its attribution to the operational period. While some uncertainty is inherent to this approach, the magnitude of the associated error remains difficult to quantify. It is unlikely that our approach alters the overall interpretation of burial as a dominant component of the carbon budget. Future studies incorporating geochronological techniques will help to further estimate burial rates more precisely. Lastly, the annual net carbon budget of the saltern was estimated based on the integration of carbon flux rates and sedimentary burial rates over very different time scales, which may be an additional source of error. Fluxes were extrapolated to annual rates based on hourly rates, whereas sedimentary carbon burial was extrapolated to annual rates based on the carbon accumulated over a period of 49 years, because the last major reconfiguration of the saltern. Minor sources of uncertainty in our budget may also arise from the potential linkage between air-water CO_2 uptake and the subsequent accumulation of OM in the sediment, which may introduce some degree of overlap between these flux components.

5. Conclusions

In summary, carbon sequestration rates per unit area in the Ria Formosa saltern were lower than coastal vegetated blue carbon systems, but as opposed to them, there was a net annual uptake of CO_2 that largely offsets the CH_4 emissions. This and the substantial amount of carbon sequestered in the sediments render the studied Ria Formosa saltern a relevant "White Carbon" sink of 1.49–3.16 Mg CO_2-eq yr^{-1}. This suggests that the sea-salt industry may function as a carbon sink as opposed to other coastal industries such as fish and shrimp aquaculture (Xu et al., 2023). Future studies with additional measurements across a wider range of salterns are needed to evaluate the relevance of "white carbon."

Conflict of Interest

The authors declare no conflicts of interest relevant to this study.

Availability Statement

The data set generated in this study is available in Zenodo (de los Santos & Alexandre, 2026, https://doi.org/10.5281/zenodo.17867948). SigmaPlot 16 (2024) and Sci-Crunch (RRID: SCR_003210) were used for data analysis and to produce manuscript's Figures 3 and 4 (registration is required). R Core Team, 2023 version 4.3.1 was used for statistical analysis of sedimentary carbon data and to produce Figures 5–7.

Acknowledgments
We are very thankful to the NECTON staff and G. Bocelli for their support during the execution of the field work. We also thank the anonymous reviewers for their constructive comments, which greatly improved the quality of the manuscript. This study received Portuguese national funds from FCT - Foundation for Science and Technology through contracts UID/04326/2025, UID/PRR/04326/2025 and LA/P/0101/2020, and through contract program DL57/2016/CP1361/CT0001 (A.A.), contract 2020.03825.CEECIND (C.B.d.l.S.), contract 2020.01282.CEECIND (N.S.) and PhD Grants 2020.06996.BD (M.M.) and 2022.11198.BD (F.P.). Open access publication funding provided by FCT (b-on).

References

Al-Haj, A. N., & Fulweiler, R. W. (2020). A synthesis of methane emissions from shallow vegetated coastal ecosystems. *Global Change Biology*, *26*(5), 2988–3005. https://doi.org/10.1111/gcb.15046

Asplund, M. E., Bonaglia, S., Boström, C., Dahl, M., Deyanova, D., Gagnon, K., et al. (2022). Methane emissions from Nordic seagrass meadow sediments. *Frontiers in Marine Science*, *8*, 811533. https://doi.org/10.3389/fmars.2021.811533

Bahlmann, F., Weinberg, I., Lavrič, J. V., Eckhardt, T., Michaelis, W., Santos, R., & Seifert, R. (2015). Tidal controls on trace gas dynamics in a seagrass meadow of the Ria Formosa lagoon (southern Portugal). *Biogeosciences*, *12*(6), 1683–1696. https://doi.org/10.5194/bg-12-1683-2015

Baxevanis, A. D., El-Bermawi, N., Abatzopoulos, T. J., & Sorgeloos, P. (2004). Salinity effects on maturation, reproductive and life span characteristics of four Egyptian Artemia populations (international study on Artemia. LXVIII). *Hydrobiologia*, *513*(1–3), 87–100. https://doi.org/10.1023/B:hydr.0000018174.72317.cf

Bianchi, T. S. (2007). *Biogeochemistry of estuaries*. Oxford University Press. 704. https://doi.org/10.1093/oso/9780195160826.001.0001

Brown, D. R., Marotta, H., Peixoto, R. B., Enrich-Prast, A., Barroso, G. C., Soares, M. L. G., et al. (2021). Hypersaline tidal flats as important "blue carbon" systems: A case study from three ecosystems. *Biogeosciences*, *18*(8), 2527–2538. https://doi.org/10.5194/bg-18-2527-2021

Browne, R. A., Davis, L. E., & Sallee, S. E. (1988). Effects of temperature and relative fitness of sexual and asexual brine shrimp Artemia. *Journal of Experimental Marine Biology and Ecology*, *124*(1), 1–20. https://doi.org/10.1016/0022-0981(88)90201-8

Castillo, J. A. A., Apan, A. A., Maraseni, T. N., & Salmo, S. G. (2017). Soil C quantities of mangrove forests, their competing land uses, and their spatial distribution in the coast of Honda Bay, Philippines. *Geoderma*, *293*, 82–90. https://doi.org/10.1016/j.geoderma.2017.01.025

de los Santos, C. B., & Alexandre, A. (2026). Data from: White is a new shade of blue carbon: A case Study of a traditional salt production pond that is a net carbon sink [Dataset]. *Zenodo*. https://doi.org/10.5281/zenodo.17867948

Díaz-Almela, E., Piñeiro-Juncal, N., Marco-Méndez, C., Giralt, S., Leiva-Dueñas, C., & Mateo, M. A. (2019). Carbon stocks and fluxes associated to Andalusian salt marshes. *Deliverable C2.2, Project LIFE Blue Natura (LIFE14CCM/ES/000957), UICN*, *2*(April), 84. https://life-bluenatura.eu/wp-content/uploads/2017/01/LIFE-Blue-Natura_Entregable-C2_Final_low.pdf

Diefenderfer, H. L., Cullinan, V. I., Borde, A. B., Gunn, C. M., & Thom, R. M. (2018). High-frequency greenhouse gas flux measurement system detects winter storm surge effects on salt marsh. *Global Change Biology*, *24*(12), 5961–5971. https://doi.org/10.1111/gcb.14430

Dooling, G. P., Chapman, P. J., Baird, A. J., Shepherd, M. J., & Kohler, T. (2018). Daytime-only measurements underestimate CH_4 emissions from a restored bog. *Écoscience*, *25*(3), 259–270. https://doi.org/10.1080/11956860.2018.1449442

Douglas, E. J., Lam-Gordillo, O., Hailes, S. F., Lohrer, A. M., & Cummings, V. J. (2025). Simulated heatwave alters intertidal estuary greenhouse gas fluxes. *Nature Communications*, *16*(1), 10507. https://doi.org/10.1038/s41467-025-65519-z

Ferrón, S., Ortega, T., Gómez-Parra, A., & Forja, J. M. (2007). Seasonal study of dissolved CH_4, CO_2 and N_2O in a shallow tidal system of the bay of Cádiz (SW Spain). *Journal of Marine Systems*, *66*(1–4), 244–257. https://doi.org/10.1016/j.jmarsys.2006.03.021

Ganning, B., & Wulff, F. (1969). The effects of bird droppings on chemical and biological dynamics in brackish water rockpools. *Oikos*, *20*(2), 274–286. https://doi.org/10.2307/3543194

George, R., Gullström, M., Mtolera, M. S. P., Lyimo, T. J., & Björk, M. (2020). Methane emission and sulfide levels increase in tropical seagrass sediments during temperature stress: A mesocosm experiment. *Ecology and Evolution*, *10*(4), 1–12. https://doi.org/10.1002/ece3.6009

Gulliver, A., Carnell, P. E., Trevathan-Tackett, S. M., Duarte De Paula Costa, M., Masqué, P., & Macreadie, P. I. (2020). Estimating the potential Blue Carbon gains from tidal marsh rehabilitation: A case study from South Eastern Australia. *Frontiers in Marine Science*, *7*, 403. https://doi.org/10.3389/fmars.2020.00403

Holmer, M., & Kristensen, E. (1994). Coexistence of sulfate reduction and methane production in an organic-rich sediment. *Marine Ecology Progress Series*, *107*, 177–184. https://doi.org/10.3354/meps107177

Howard, J., Hoyt, S., Isensee, K., Pidgeon, E., & Telszewski, M. (Eds.) (2014). *Coastal Blue Carbon: Methods for assessing carbon stocks and emission factors in mangroves, tidal salt marshes, and seagrass meadows*. Conservation International, Intergovernmental Oceanographic Commission of UNESCO, International Union for Conservation of Nature.

Huertas, I. E., Paz, M., Perez, F. F., Navarro, G., & Flecha, S. (2019). Methane emissions from the salt marshes of Doñana wetlands: Spatio-temporal variability and controlling factors. *Frontiers in Ecology and Evolution*, *7*, 32. https://doi.org/10.3389/fevo.2019.00032

Instituto Português do Mar e da Atmosfera, Data Clima. (2026) Retrieved from https://dataclima.ipma.pt, accessed in January 2026.

IPCC. (2021). In V. Masson-Delmotte, P. Zhai, A. Pirani, S. L. Connors, C. Péan, et al. (Eds.), *Climate change 2021: The physical science Basis. Contribution of Working Group I to the sixth assessment report of the intergovernmental Panel on climate change*. Cambridge University Press. https://doi.org/10.1017/9781009157896

Iram, N., Kavehei, E., Maher, D. T., Bunn, S. E., Rashti, M. R., Farahani, B. S., & Adame, M. F. (2021). Soil greenhouse gas fluxes from tropical coastal wetlands and alternative agricultural land uses. *Biogeosciences*, *18*(18), 5085–5096. https://doi.org/10.5194/bg-18-5085-2021

Jähne, B. (2019). Air-sea gas exchange. In J. K. Cochran, H. J. Bokuniewicz, & P. L. Yager (Eds.), *Encyclopedia of Ocean Sciences* (Vol. 6, pp. 1–13). Academic Press. https://doi.org/10.1016/B978-0-12-409548-9.11613-6

Keneally, C., Southgate, M., Chilton, D., Gaget, V., Welsh, D. T., Mosley, L., et al. (2024). Organic matter accumulation drives methylotrophic methanogenesis and microbial ecology in a hypersaline coastal lagoon. *Limnology and Oceanography*, *69*(9), 1970–1983. https://doi.org/10.1002/lno.12637

Lovelock, C. E., & Duarte, C. M. (2019). Dimensions of blue carbon and emerging perspectives. *Biology Letters*, *15*(3), 20180781. https://doi.org/10.1098/rsbl.2018.0781

Ma, T., Li, X., Bai, J., Ding, S., Zhou, F., & Cui, B. (2019). Four decades' dynamics of coastal blue carbon storage driven by land use/land cover transformation under natural and anthropogenic processes in the yellow River Delta, China. *Science of The Total Environment*, *655*, 741–750. https://doi.org/10.1016/j.scitotenv.2018.11.287

Martins, M., de los Santos, C. B., Masqué, P., Carrasco, A. R., Veiga-Pires, C., & Santos, R. (2022). Carbon and nitrogen stocks and burial rates in intertidal vegetated habitats of a mesotidal coastal lagoon. *Ecosystems*, *25*(2), 372–386. https://doi.org/10.1007/s10021-021-00660-6

Maxwell, T. L., Rovai, A. S., Adame, M. F., Adams, J. B., Álvarez-Rogel, J., Austin, W. E. N., et al. (2023). Global dataset of soil organic carbon in tidal marshes. *Scientific Data*, *10*(1), 797. https://doi.org/10.1038/s41597-023-02633-x

McGenity, T. J., & Sorokin, D. Y. (2019). Methanogens and methanogenesis in hypersaline environments. In A. Stams & D. Sousa (Eds.), *Biogenesis of hydrocarbons. Handbook of hydrocarbon and lipid microbiology*. Springer. https://doi.org/10.1007/978-3-319-78108-2_12

Neubauer, S. C., Franklin, R. B., & Berrier, D. J. (2013). Saltwater intrusion into tidal freshwater marshes alters the biogeochemical processing of organic carbon. *Biogeosciences*, *10*(12), 8171–8183. https://doi.org/10.5194/bg-10-8171-2013

Poffenbarger, H. J., Needelman, B. A., & Megonigal, J. P. (2011). Salinity influence on methane emissions from tidal marshes. *Wetlands*, *31*(5), 831–842. https://doi.org/10.1007/s13157-011-0197-0

Ramjattan, K. (2022). *A meta-analysis of the carbon ecosystem service in human-managed coastal environments*. University of Algarve. Retrieved from http://hdl.handle.net/10400.1/19853.Master Thesis.

R Core Team. (2023). R: A Language and environment for statistical computing [Software]. R Foundation for Statistical Computing. Retrieved from https://www.R-project.org/

Rodriguez, K., Ricci, F., Ni, G., Iram, N., Palfreyman, R. A., Gonzalez-Garcia, R. A., et al. (2025). Abundant and active acetogens enhance the carbon dioxide sink of Blue carbon ecosystems. *bioRxiv*, *2025–01*. https://doi.org/10.1101/2025.01.07.631696

Roth, F., Broman, E., Sun, X., Bonaglia, S., Nascimento, F., Prytherch, J., et al. (2023). Methane emissions offset atmospheric carbon dioxide uptake in coastal macroalgae, mixed vegetation and sediment ecosystems. *Nature Communications*, *14*(1), 42. https://doi.org/10.1038/s41467-022-35673-9

Schulz, K. G., Bach, L. T., & Dickson, A. G. (2023). Seawater carbonate chemistry considerations for ocean alkalinity enhancement research: Theory, measurements, and calculations. *State Planet, 2-oae2023*, *2*, 1–14. https://doi.org/10.5194/sp-2-oae2023-2-2023

Segers, R. (1998). Methane production and methane consumption: A review of processes underlying wetland methane fluxes. *Biogeochemistry*, *41*(1), 23–51. https://doi.org/10.1023/A:1005929032764

Sieczko, A., Duc, N. T., Schenk, D., Pajala, G., Rudberg, D., Sawakuchi, H. O., & Bastviken, D. (2020). Diel variability of methane emissions from lakes. *PNAS*, *117*(35), 21489–21494. https://doi.org/10.1073/pnas.2006024117

SigmaPlot 16 (RRID:SCR_003210). (2024). SigmaPlot 16 (RRID:SCR_003210) statistical analysis and scientific graphing software for Windows OS [Software]. *Grafiti LLC*. Retrieved from http://www.sigmaplot.com/products/sigmaplot/

Soares, R. H. R. M., Assunção, C. A., Fernandes, F. O., & Marinho-Soriano, E. (2018). Identification and analysis of ecosystem services associated with biodiversity of saltworks. *Ocean and Coastal Management*, *163*, 278–284. https://doi.org/10.1016/j.ocecoaman.2018.07.007

Sripanomyom, S., Round, P. D., Savini, T., Trisurat, Y., & Gale, G. A. (2011). Traditional salt-pans hold major concentrations of overwintering shorebirds in Southeast Asia. *Biological Conservation*, *144*(1), 526–537. https://doi.org/10.1016/j.biocon.2010.10.008

Susano, C. L., & Gonçalves, M. M. (2020). Salt: The white gold of Algarve. In *Rehabend Congress, construction pathology*. Rehabilitation Technology and Heritage Management. Retrieved from https://www.researchgate.net/publication/344407437

Takekawa, J. Y., Miles, A. K., Schoellhamer, D. H., Athearn, N. D., Saiki, M. K., Duffy, W. D., et al. (2006). Trophic structure and avian communities across a salinity gradient in evaporation ponds of the San Francisco Bay estuary. *Hydrobiologia*, *567*, 307–327.

Thomas, A. D., Dougill, A. J., Elliott, D. R., & Mairs, H. (2014). Seasonal differences in soil CO_2 efflux and carbon storage in Ntwetwe Pan, Makgadikgadi Basin, Botswana. *Geoderma*, *219–220*, 72–81. https://doi.org/10.1016/j.geoderma.2013.12.028

Vieira, S., Ribeiro, L., Silva, J. M., & Cartaxana, P. (2013). Effects of short-term changes in sediment temperature on the photosynthesis of two intertidal microphytobenthos communities. *Estuarine, Coastal and Shelf Science*, *119*, 112–118. https://doi.org/10.1016/j.ecss.2013.01.001

Wanninkhof, R., & Triñanes, J. (2017). The impact of changing wind speeds on gas transfer and its effect on global air-sea CO_2 fluxes. *Global Biogeochemical Cycles*, *31*(6), 961–974. https://doi.org/10.1002/2016GB005592

Weston, N. B., Neubauer, S. C., Velinsky, D. J., & Vile, M. A. (2014). Net ecosystem carbon exchange and the greenhouse gas balance of tidal marshes along an estuarine salinity gradient. *Biogeochemistry*, *120*(1–3), 163–189. https://doi.org/10.1007/s10533-014-9989-7

Xu, C., Su, G., Zhao, K., Wang, H., Xu, X., Li, Z., et al. (2023). Assessment of greenhouse gases emissions and intensity from Chinese marine aquaculture in the past three decades. *Journal of Environmental Management*, *329*, 117025. https://doi.org/10.1016/j.jenvman.2022.117025

Yang, W., Yuan, S., Huang, B., Tong, C., & Yang, L. (2018). Emission characteristics of greenhouse gases and their correlation with water quality at an estuarine mangrove ecosystem – The application of an in-situ on-site NDIR monitoring technique. *Wetlands*, *38*(4), 723–738. https://doi.org/10.1007/s13157-018-1015-8

Yau, Y. Y. Y., Reithmaier, G., Majtényi- Hill, C., Serrano, O., Piñeiro-Juncal, N., Dahl, M., et al. (2023). Methane emissions in seagrass meadows as a small offset to carbon sequestration. *Journal of Geophysical Research: Biogeosciences*, *128*(6), e2022JG007295. https://doi.org/10.1029/2022JG007295

Yu, J., Wang, Y., Li, Y., Dong, H., Zhou, D., Han, G., et al. (2012). Soil organic carbon storage changes in coastal wetlands of the modern Yellow River Delta from 2000 to 2009. *Biogeosciences*, *9*(6), 2325–2331. https://doi.org/10.5194/bg-9-2325-2012

Yusup, Y., Swesi, A. E., Sigid, M. F., Almdhun, H. M., & Jamshidi, E. J. (2023). The relationship between carbon dioxide flux and environmental parameters at a tropical coastal sea on different timescales. *Marine Pollution Bulletin*, *193*, 115106. https://doi.org/10.1016/j.marpolbul.2023.115106

Yvon-Durocher, G., Allen, A. P., Bastviken, D., Conrad, R., Gudasz, C., St-Pierre, A., et al. (2014). Methane fluxes show consistent temperature dependence across microbial to ecosystem scales. *Nature*, *507*(7493), 488–491. https://doi.org/10.1038/nature13164

Zhang, Y., Yang, P., Wang, Y., Zhao, G., Zheng, Z., Zou, Y., et al. (2024). Rainstorm and strong wind weathers largely increase greenhouse gases flux in shallow ponds. *Science of the Total Environment*, *923*, 171478. https://doi.org/10.1016/j.scitotenv.2024.171478

Zhang, Z., Poulter, B., Feldman, A. F., Ying, Q., Ciais, P., Peng, S., & Li, X. (2023). Recent intensification of wetland methane feedback. *Nature Climate Change*, *13*(5), 430–443. https://doi.org/10.1038/s41558-023-01629-0

Zhou, J., Theroux, S. M., Mesquita, C. P. B., Hartman, W. H., Tian, Y., & Tringe, S. G. (2021). Microbial drivers of methane emissions from unrestored industrial salt ponds. *The ISME Journal*, *16*(1), 284–295. https://doi.org/10.1038/s41396-021-01067-w